sciendo DOI: 10.2478/ace-2018-0018 ARCHIVES OF CIVIL ENGINEERING
Vol. LXIV ISSUE 2 2018

EXPERIMENTAL STUDY OF MULTI-RIBBED ONE-WAY COMPOSITE SLABS MADE OF STEEL FIBRE, FOAM, AND NORMAL CONCRETE

YABO WANG [1], H. T. LIU[2], G. F. DOU[3], C. H. XI[4], L. QIAN[5]

Abstract: This paper aims to study the effect of reinforcement configuration (steel fibre and rebar) on the mechanical performance of composite slabs of the same total steel contents. We manufactured four pieces of full-scale multi-ribbed composite prefabricated slabs with different reinforcement configurations by using steel fibre-reinforced concrete, foam concrete, and normal concrete. The multi-ribbed composite prefabricated slab has many excellent properties, such as light weight, good thermal and sound insulation. Thus, it can be applied to fabricated structures. In addition, the composite prefabricated slabs with the same total steel contents but with different reinforcement configurations were studied under the same static load, and many technical indicators such as crack resistance capacity, yield load, ultimate load capacity, maximum deflection, destructive pattern, and stress of steel rebar were obtained. Results indicate reinforcement configuration has a significant effect on the mechanical performance of composite prefabricated slabs with the same total steel contents, and composite prefabricated slabs reinforced with longitudinal rebar and steel fibre (volume fraction is 1.5%) have the best mechanical performance and ductility.

Keywords: steel fibre, foam concrete, multi-ribbed slab, one-way slab, composite slab

[1] Assoc. Prof., PhD., Eng., Jilin Jianzhu University, Jilin Structure and Earthquake Resistance Technology Innovation Center, Changchun 130118, China, e-mail: wangyabo@jlju.edu.cn
[2] PhD., Eng., Jilin Jianzhu University, Jilin Structure and Earthquake Resistance Technology Innovation Center, Changchun 130118, China, e-mail: academic_365@outlook.com
[3] PhD., Eng., Jilin Jianzhu University, Jilin Structure and Earthquake Resistance Technology Innovation Center, Changchun 130118, China, e-mail: albert.brook@outlook.com
[4] PhD., Eng., Jilin Jianzhu University, Jilin Structure and Earthquake Resistance Technology Innovation Center, Changchun 130118, China, e-mail: cooper.well@outlook.com
[5] PhD., Eng., Jilin Jianzhu University, Jilin Structure and Earthquake Resistance Technology Innovation Center, Changchun 130118, China, e-mail: uranium_235@163.com

1. INTRODUCTION

The addition of fibre into concrete can increase crack resistance, tensile strength, and stiffness. Thus, there are many codes providing guidelines for its design [1–4]. Glass fibre [5], steel fibre [6–11], plastic fibre [12], carbon fibre [13, 14], as well as others can be used as reinforcing material for concrete. Steel fibre has been studied as a kind of material enhancing the flexural strength of self-compacting concrete sheets [15–17]. Foam concrete, which has many excellent properties including light weight and good thermal insulation, is widely used as a material of walls, roofs, and flooring [18]. However, because foam concrete has high water absorption capacity, it has poor frost resistance after absorbing water and can easily break during freeze-thaw cycles. In contrast, steel fibre-reinforced concrete has good crack resistance and impermeability [19]. Thus, combining the advantages of steel fibre reinforced concrete (good impermeability) and multi-ribbed structures (good mechanical performance), we designed a new type of multi-ribbed prefabricated composite slab. This composite slab uses foam concrete as the core layer, steel fibre-reinforced concrete as the surficial layer, and rebar-reinforced concrete as the ribs.

Steel fibre-reinforced concrete has been widely used in the construction industry. Some researchers think that it can improve the overall strength and flexural strength of structures [20, 21]. With the addition of steel fibre into the member, the ductility of the member and its tension redistribution ability after cracking can be significantly improved. With a simultaneous addition of continuously deformed rebar and randomly distributed steel fibres into concrete, the hybrid steel fibre-rebar-reinforced concrete can be obtained, attaining the best structure [22–26]. When the volume content of the steel fibre in this hybrid material reaches 60 kg/m^3, the crack resistance of it can be significantly improved; it is then higher than that of the steel mesh-reinforced concrete [27].

In this paper, we studied the effect of reinforcement configuration (steel fibre and rebar) on the mechanical performance of composite slabs and obtained the optimum reinforcement configuration. The manufacturing process of composite slabs is more complicated than that of normal concrete slabs. However, composite slabs have good mechanical performance, high crack resistance, good thermal insulation, and low-cost operation and maintenance, which satisfies the requirements of industrialization of structural members, building energy efficiency, and “green” buildings. Thus, despite its complex manufacturing process, this kind of composite slab has bright market prospects and broad applications.

2. EXPERIMENT DESIGN

2.1. PROPERTY TESTING

2.1.1. STRENGTH OF STEEL FIBRE-REINFORCED CONCRETE AND PLAIN CONCRETE

According to the guideline [28], three groups of cubic blocks were made for the common concrete and steel fibre concrete, respectively. Each group included six test blocks, and the size of the test block was 150 mm × 150 mm × 150 mm. After 28 days of nurture under the same conditions, the average compressive strengths of the cubic steel fibre-reinforced concrete blocks and plain concrete blocks were 38.7 MPa and 39.54 MPa, respectively.

2.1.2. PROPERTIES OF REBAR

We tested the properties of HPB 300 and HPB 400 rebar and obtained the following results (each value is the mean of six rebar samples): the ultimate strength of HPB300 rebar is 624 MPa and its total elongation rate is 17.5%; the ultimate strength of HRB400 rebar is 618 MPa and its total elongation rate is 13.5%. These values meet the requirements of the code; that is, the total elongation rates of HPB300 and HRB400 rebar should be no less than 10% and 7.5%, respectively.

2.2. DESIGN AND MANUFACTURE OF SLABS

The design principle in this experiment is that all slabs are of the same total steel content (calculated through the equal strength principle). To investigate the effects of different reinforcement configurations (steel fibre and rebar) on the mechanical performance of composite prefabricated slabs, four experimental slabs were designed. B1: Both the tensile and compressive layer use steel fibre-rebar-reinforced concrete (volume fraction of the steel fibre is 1.5%). The core layer uses foam concrete composite slabs with a density of 200 kg/m^3. B2: Both the tensile and compressive layer use rebar-reinforced concrete. The core layer uses foam concrete composite slabs with a density of 200 kg/m^3. B3: Both the tensile and compressive layer use steel fibre-reinforced concrete (volume fraction is 2.0%). The core layer uses foam concrete composite slabs with a density of 200 kg/m^3. B4: The tensile layer uses steel fibre-rebar-reinforced concrete (volume fraction of the steel fibre is 1.5%). Both the compressive layer and the core layer use foam concrete composite slabs with a density of

700 kg/m^3. All experimental slabs have the same size, with a length of 3600 mm, a width of 1200 mm, a height of 120 mm, rib beam height of 80 mm, and rib width of 60 mm.

As shown in Figure 1, the peripheral border line and the internal dotted line represent ribs in the experimental slabs. Steel fibre-reinforced concrete is of C30 class and the manufacturing process uses normal Portland cement (42.5), river sand (fineness modulus is 2.5–2.7), crushed stone maximum diameter ≤ 20 mm, average diameter = 15 mm), first-class silica fume, copper tailings ground by a metallurgical slag plant, and sheared steel fibres with a length of 30 mm, a diameter of 0.8mm, an ultimate tensile strength of 700 MPa, and a yield strength of 450 MPa (Anshan Kebite Co., Ltd., Anshan, China).

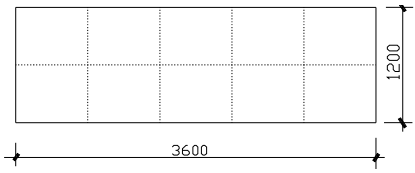

Fig. 1. Plan View of B1–B4.

The rebar reinforcement of B1–B4 is shown in Figures 2-5, respectively. B1–B4 were modelled in a prefabricated factory (ChangChun, China), nurtured naturally for 28 days, and transported to the Civil Engineering Laboratory of Jilin Architecture University. The B in B1–B4 represents composite slab and the numbers 1, 2, 3, and 4 represent slabs with different reinforcement configurations. As mentioned above, the total steel content in all four experimental slabs is the same and was calculated through the equal strength principle. The amounts of total steel and reinforcement of the experimental slabs are shown in Table 1.

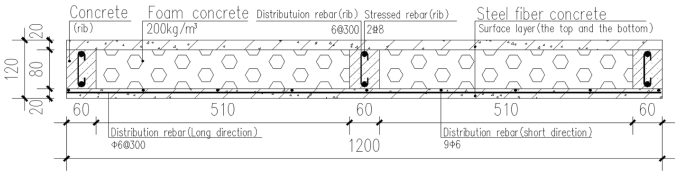

Fig. 2. Sectional View of B1.

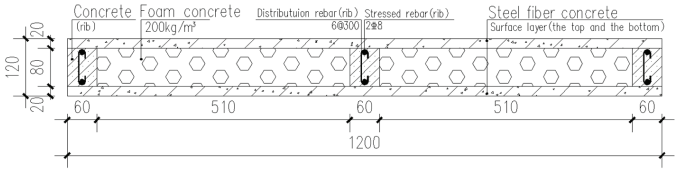

Fig. 3. Sectional View of B2.

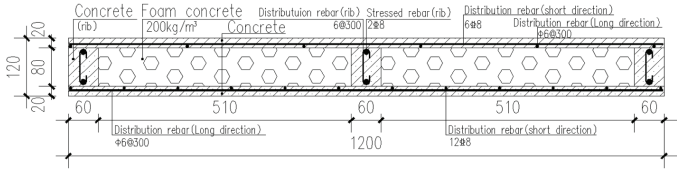

Fig. 4. Sectional View of B3.

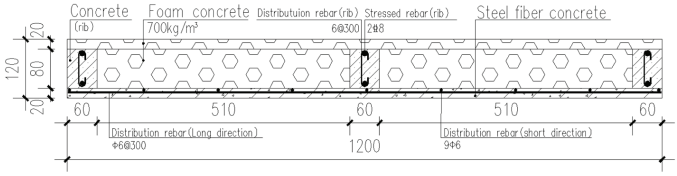

Fig. 5. Sectional View of B4.

Table 1. Materials and Reinforcement Ratio for Experimental Slabs.

Slab			**B1**	**B2**	**B3**	**B4**
The thickness of bottom surface (20 mm)	The class of the based materials and rebar	Concrete	C30 (V_f = 1.5%)	C30	C30 (V_f = 2.0%)	C30 (V_f = 1.5%)
		Rebar	HPB300	Long side: HRB400; Short side: HPB300	-	HPB300
	Reinforcement	Force on the long side	9 with d = 6 mm	12 with d = 8 mm	-	9 with d = 6 mm
		Distribution of the short side	d= 6 mm; gap = 300 mm	d= 6 mm; gap = 300 mm	-	d = 6 mm; gap = 300 mm
		Longitudinal rebar ratio (%)	0.2	0.46	0	0.2
The thickness of top surface (20 mm)	The class of the based materials and rebar	Concrete	C30 (V_f = 1.5%)	C30	C30 (V_f = 2.0%)	foam concrete (ρ= 700 kg/m^3)
		Rebar	-	Long side:HRB400; Short side: HPB300	-	-
	Reinforcement	Force on the long side	-	six with d = 8 mm	-	-
		Distribution of the short side	-	d = 6 mm; gap = 300 mm	-	-
Rib (60 mm × 80 mm)	The class of the based materials and rebar	Concrete	C30	C30	C30	C30
		Rebar	Longitudinal reinforcement HRB400; Stirrup HPB300	Longitudinal reinforcement HRB400; Stirrup HPB300	Longitudinal reinforcement HRB400; Stirrup HPB300	Longitudinal reinforcement HRB400; Stirrup HPB300
	Reinforcement	Longitudinal rebar	two with d = 8 mm	two with d = 8 mm	two with d = 8 mm	two with d = 8 mm
		Stirrup	d = 6 mm; gap = 300 mm	d = 6 mm; gap = 300 mm	d= 6 mm; gap = 300 mm	d = 6 mm; gap = 300 mm
Materials of the core	Density of foam concrete (kg/m^3)		200	200	200	700
The total steel content (kg)			36	48	43	36

2.2.1. Loading and Measuring Points

In this experiment, the flexural performances of B1–B4 were investigated under vertical static load. An eight-point loading program of counter-force beam two-step loading was adopted [28]. Under the current experimental conditions, the experimental slabs can hardly be destroyed under a uniformly distributed load. However, the thickness of the surface layer of each slab is only 20 mm, and as that cannot bear the concentrated load the loading plan was changed so that the load acts on the intersectional points of the longitudinal rib and the transverse rib. A hydraulic loading system was used; the jack was calibrated to obtain a specific load–displacement relationship, and manual loading was adopted. The loading value can be obtained from a strain gauge connected to the hydraulic pressure sensor. The loading device is shown in Figure 6. A plastic pad with a diameter of 400 mm and thickness of 100 mm was placed at the loading position.

Fig. 6. The Loading Device.

Before loading, preloading was performed to ensure that the experimental structural member would work properly during loading. It can check whether the loading device and instruments work properly and also compact the support. The preload for B1–B4 is 5 kN. It should be noted that the preload cannot be higher than 30% of the cracking load of a structural member. After this operation the preload was totally removed, and after the structure members had been fully recovered, loading was performed. Static destruction experiments were performed on B1–B4, and the process is defined as 6–19 level loading according to the cracking load, working load, and ultimate load of these experimental slabs. When the loading was performed, the load at each level was adjusted according to the actual situation, and each level of loading lasted 10 min. When the specimen was near cracking, the load at each level fell by half; when the cracking load was reached, the load at each level increased to its original value; when the load on the specimen almost reached the ultimate load, the load at each level should not be greater than 0.05 times the ultimate load. During the process the tension and strain of the slabs were recorded. The weight of the slab and the loading device are a part of the load in this experiment. After a stable deformation of experimental slabs was achieved at each level of loading,

the deflection value was calculated through multiplying the deflection value obtained from the displacement gauge and the strain gauge by a correction factor, which is 0.94 in this experiment [28]. Vertical displacement gauges were placed at the midspan of the slab. There were two displacement gauges placed at each position, and the mean of the values obtained from them was used. The distribution of the rebar strain gauges is shown in Figure 7, and the distribution of the strain gauges for concrete is shown in Figure 8. Meanwhile, the crack extension, deformation, and destructive characteristics of the slabs were observed and recorded.

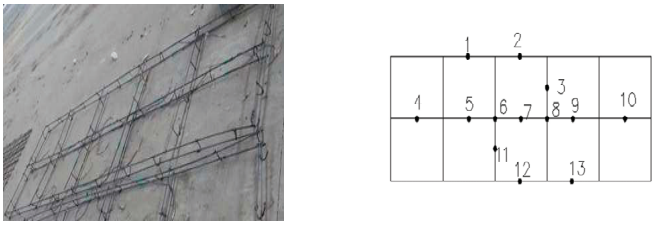

Fig. 7. Distribution of Rebar Strain Gauges.

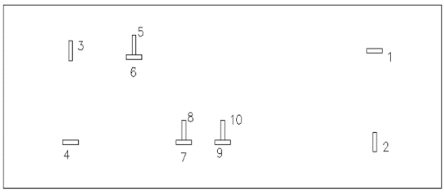

Fig. 8. Distribution of Strain Gauges for Concrete.

3. RESULTS AND DISCUSSION

3.1. LOAD–DEFLECTION ANALYSIS

3.1.1. DATA

Table 2. Experimental Data.

Slab	Cracking load (kN)	Yield load (kN)	Ultimate load (kN)	Deflection of slab under ultimate load (mm)	Ultimate deflection of slab (mm)
B1	26	42	53	40	60
B2	20	46	59	38	51
B3	10	-	12	8	14
B4	26	38	44	38	42

Note: the ultimate deflection is the maximum deflection at the geometric center of the test floor.

3.1.2. DATA ANALYSIS

A. Cracking load

Before the cracking loads of the experimental slabs were reached, the experimental slabs were in their elastic stage, their P–Δ curves are almost coincident, and their deflections are close to each other. Because the load was applied to the slab manually and gradedly, the cracking load of the slab was usually coincident with its load grading. In addition, as shown in the P–Δ curves for B1 and B4, the change in the slope near the cracking load is insignificant, so it is difficult to accurately determine the cracking loads of B1 and B4. As shown in the P–Δ curve for B2, B2 has a four-stage working state, thus it is relatively easy to determine the cracking load of B2. For B3, there is large deformation when it cracks, and then it is destroyed (Figure 9).

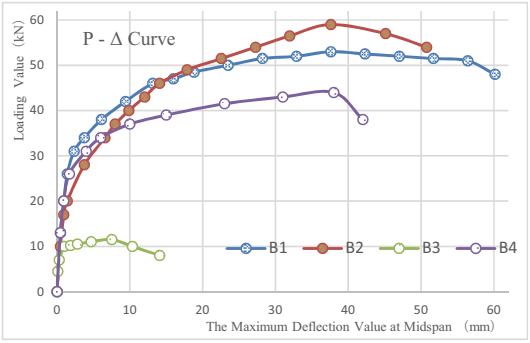

Fig. 9. Load–Deflection Curves for Four Experimental Slabs at Midspan.

Although the total steel contents in B1–B4 are the same, the cracking loads of the four experimental slabs are different. The cracking load of B3 is the lowest, followed by B2, and the cracking loads of B1 and B4 are the highest - close to each other and 23% higher than that of B2. This implies that at a proper volumetric reinforcement ratio steel fibre in a slab can help resist cracking and improve crack resistance and cracking load. However, when a high volumetric fraction of steel fibre is added to the slab which is not reinforced with rebar, its cracking load is not improved and remains close to that of plain concrete. The test specimen also shows obvious characteristics of brittle fracture.

B. Normal working stage

The loading–deflection curve at the midspan of each slab is shown in Figure 9.

When entering the elastic stage, B2 has an obvious turning point, while B1 and B4 change only insignificantly. There are decreases in the stiffness of B1, B2, and B4, and that of B2 is the most

significant. This means that the slope of the P – △ curve for B2 is smaller than those for B1 and B4. When the loads on B1, B2, and B4 reach 42 kN, 46 kN, and 38 kN, respectively, their deflections begin to increase rapidly. Then, these members enter into their plastic stages. When the rebar yields, the bearing capacity of B2 is the highest, about 10%, and 21% higher than those of B1 and B4, respectively. B3 destructs after cracking, so it has no normal operational stage.

C. Ultimate load

The deflection of B3 reaches its ultimate value first. After cracking, the bearing capacity of B3 barely increases, but the deflection increases significantly, showing obvious characteristics of brittle fracture. The ultimate load of B3 is 12 kN. The ultimate loads of B1, B2, and B4 are 53 kN,59 kN, and 44 kN, respectively. When ultimate loads are reached, as the load decreases the deflections of B1, B2, and B4 still increase, their ultimate deflections are 60 mm, 51 mm, and 42 mm, respectively. The yield load and ultimate load of B2 are the highest because the longitudinal rebar content of B2 is the highest. Although the volume fraction of steel fibre and rebar reinforcement in the tensile layers of B1 and B4 are the same, light foam concrete in the compressive layer of B4 creases before the yield load is reached because of its low strength. Then, the foam concrete is crushed and B4 is destroyed with excessive deformation. Thus, the ultimate load of B4 is lower than that of B1. The top surface and bottom of B1 are steel fibre-rebar-reinforced concrete, so the ultimate bearing capacity of it is higher than that of B4. In addition, the amount of longitudinal rebar reinforcement in B1 is lower than that in B2, so the ultimate bearing capacity of B1 is lower than that of B2.

D. Stiffness

B1 does not meet the requirements of the minimum rebar reinforcement ratio as described in the Concrete Structural Design code [29], so it is a kind of less-reinforced slab. However, as the P – △ curve shows, B1 does not show characteristics of brittle fracture, which a less-reinforced slab often has, and B1 has good ductility. Therefore, when total steel content in concrete is fixed to a specific value, increasing steel fibre content (but decreasing deformed rebar content) cannot improve working load and ultimate bearing capacity of the concrete. However, the addition of steel fibre into rebar-reinforced concrete can significantly improve the ductility and stiffness of the concrete.

As shown by the load–displacement curves of B1–B4, before the member cracks and the rebar yields, the stiffness loss of B2 is not significant, whereas that of normal concrete is significant (Figure 10). Thus, when the displacements or the widths of cracks in the concretes are the same, the bearing capacity of steel fibre-reinforced concrete is higher than that of normal concrete. This is consistent with the results of Luca Facconi [17]. As shown in the load–deflection curve, after B1 and B2 crack, the slope of B2 is significantly smaller than that of B1, so the stiffness loss of B1 is significantly

lower than that of B2. During the loading process, B2 enters the following four stages subsequently: elastic stage, operation stage with cracks, strengthening stage, and the degenerative stage. However, the transitions between the stages of B1 and B4 are not obvious. Although B1 and B4 both undergo the elastic stage, plastic stage, strengthening stage, and the degenerative stage, the whole process is mild without a significant turning point. This indicates that the steel fibre can help bear force during the work stage of the member.

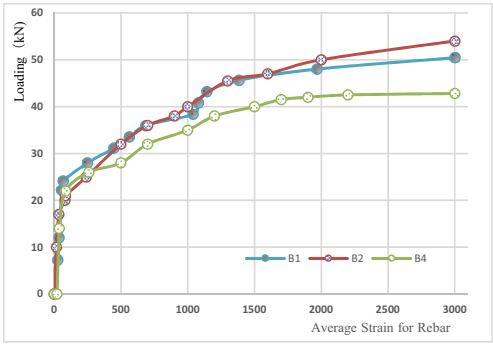

Fig. 10. The Load–Average Strain Curves for Rebars in B1, B2, and B4 at Midspan.

3.2. LOAD–STRAIN ANALYSIS

Figure 10 shows the load–average strain curve for each slab. When the load is 51kN, the strain of the rebar at the midspan of B2's bottom is 2500 με, and the corresponding tensile strength is 514 N/mm^2, which is simply the average of the measured ultimate tensile strengths of the HRB400 rebar used in B2 (514 N/mm^2). When the load is 49kN, the strain of the rebar at the midspan of B1's bottom is 2000με, and the corresponding tensile strength reaches the average of the measured ultimate tensile strengths of the HPB300 rebar used in B1 (410N/mm^2).The average of the measured yield strengths of HRB400 is 411 N/mm^2, and the average of the measured yield strengths of HPB300 is 317 N/mm^2. Both are higher than the actual yield strength. When the ultimate bearing capacity of B1–B4 is reached, the maximum strain of the rebar is about 3600με, and the rebar is in the strengthening stage. Then, as the bearing capacity decreases, the strain of the rebar still increases rapidly.

As shown in Figure 10, the trends of load–average strain curves for rebars in B1, B2, and B4 are the same. The rebar is first in its elastic stage. When the concrete cracks, the tension of the concrete acts on the rebar, resulting in a sudden increased strain of the rebar. Then, the strain of the rebar increases continuously. Finally, when the concrete reaches its yield moment, the rebar is in the plastic stage,

and then strengthening stage. Although the ultimate bearing capacities of the experimental slabs are different, the bearing capacities of all rebars reach their ultimate values.

3.3. CRACK EXTENSION AND MAXIMUM DEFLECTION

3.3.1. THE EXTENSION AND DISTRIBUTION OF CRACKS ON THE BOTTOM OF THE SLABS AND THE ULTIMATE DESTRUCTIVE STATE

During the process of loading, the crack first appears on the surface of the tensile zone. The first crack appears around the midspan of the slab because the yield moment at midspan is at its maximum. The cracks on each slab appear at the middle of its bottom and extend towards the short sides of the slabs. There is only one crack on B3, whereas there are many cracks with various patterns at different positions on B1, B2, and B4's bottoms. As the load increases, many new cracks appear symmetrically at two sides of the original crack at midspan. These cracks extend and develop along parallel lines. Finally, cracks appear near the support. Figure 11 shows the distribution of cracks at the bottoms of B1–B4. There are 11 cracks at the bottom of B1, evenly distributed within 2/3 of the slab's midspan. Every rib has a transverse long through-crack in the middle of it (besides the transverse long through-cracks at its two sides). The largest crack has a width of 5.2 mm, the deflection of B1 exceeds the ultimate value, and the maximum deflection is 60 mm. There are six cracks on bottom of B2, which are within 1/3 of the slab's midspan. The largest crack has a width of 2 mm, the deflection of B2 exceeds the ultimate value, and the maximum deflection is 51 mm. Of the four slabs, B3 cracks first. When it is destroyed, there is only one crack with a width greater than 2 mm on its bottom. Its maximum deflection is only 14 mm. The destruction of B3 shows obvious characteristics of brittle fracture. Moreover, there are only two cracks at the midspan of B4's bottom with widths greater than 2 mm. The deflection of B4 exceeds the ultimate value and the maximum deflection is 42 mm. The ductility and bearing capacity of B4 are lower than those of B1.

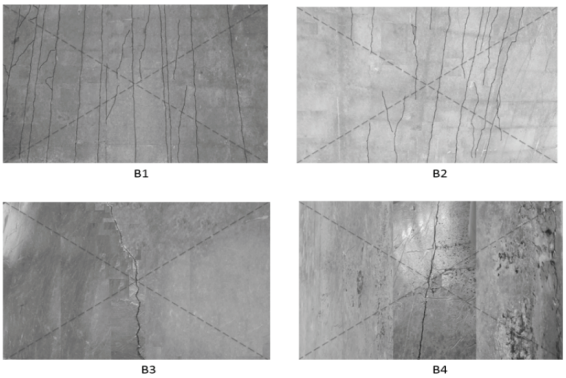

Fig. 11. Distribution of Cracks on the Bottoms of B1–B4.

3.3.2. ANALYSIS OF DESTRUCTION PHENOMENA OF SLABS

During the initial stage of loading steel fibre, concrete, and the rebar net bear the external force together. When concrete cracks, the force is transferred to the steel fibre, then the steel fibre (across the cracks) transfers the force to two sides of the cracks. This way, the materials around the cracks can still bear the load, the crack-extension rate is decreased, and a steady state of crack opening is achieved [30]. As can be seen from the destructive states of the four slabs that the highest number of cracks is on B1, they have the largest width, the most widely distributed area, and the smallest interval. After cracking, it shows the obvious characteristics of ductile destruction, and maintains the unrecovered flexural plastic state after unloading. This indicates that under a certain longitudinal rebar ratio, though it is smaller than the minimum ratio, the destructive pattern can be changed after the addition of steel fibre; that is, the brittle destructive characteristic of rebar-reinforced concrete is changed into the ductile destructive characteristic of steel fibre-rebar-reinforced concrete. The addition of the steel fibre can expand the distributed area of the cracks and reduce crack interval. This indicates that steel fibres play a major role in inhibiting cracks in concrete from further opening and they also bear part of the load. Finally, the steel fibre is snapped or pulled out from the concrete under the load (Figure 12).

When the total steel content in the slabs is the same, the cracking load of B1 is 30% higher than that of B2. The study of Luca Facconi, Fausto Minelli, Giovanni Plizzari, et al. shows that the maximum cracking load of a steel fibre-rebar-reinforced concrete sheet is 42kN (the volume fraction of steel fibre is 0.32%), whereas that of a normal rebar-reinforced concrete sheet is 31kN (both sheets measure 4200 mm × 2500 mm × 80 mm). The cracking load of the steel fibre-rebar-reinforced concrete sheet

is 35% higher than that of a traditional rebar-reinforced concrete sheet. When the amount of rebar in concrete is appropriate, the longitudinal rebar content determines the ultimate load of the concrete. B2 has the highest content of rebar, so its ultimate load is the highest, 11% higher than that of B1. In addition, inclined cracks at the supports of B1 and B3 develop more slowly than those of B2. This indicates that steel fibre in concrete can effectively transfer load around cracks. This way, inclined cracks can extend and develop, and shear resistance of concrete is improved.

Fig. 12. The Development of Cracks around Steel Fibre.

3.3.3 SOUND INSULATION AND THERMAL PERFORMANCE OF UNIDIRECTIONAL PLATE

The thermal test of foam concrete was performed in accordance with GB/T10294-2008 (the guarded hot plate apparatus method for determining steady-state thermal resistance and related properties of thermal insulation materials) [31]. Three groups of samples (300 mm × 300 mm × 30 mm) were made for the 200 kg/m^3 bulk foam concrete. Then, their thermal conductivities were determined. The average thermal conductivity of the three groups of specimens was determined to be 0.0531 W/(m·K). According to reference [32], the thermal conductivity of foam concrete with density values ranging from 200 to 700 kg/m^3 is in the range of 0.09–0.17 W/(m·K), and the thermal resistance is about 10–20 times that of ordinary concrete.

Although a sound insulation test was not conducted here, according to reference [33], foam concrete is a porous sound-absorbing material with a sound absorption coefficient of 0.8–1.4, and its sound dissipation ability can reach first or second grade standards.

It is thus clear that the composite slab made with foam concrete has not only light weight, but also good sound insulation and thermal properties.

4. CONCLUSIONS

On the basis of the mechanical analysis of these four slabs, the following conclusions can be obtained:

(1) The cracks distribute widely and evenly on B1. B1 deforms slowly and its ultimate deflection is the largest, 18%, 329%, and 43% larger than those of B2, B3, and B4, respectively. Thus, B1 exhibits excellent ductility.

(2) Although total steel content in B1–B4 is the same, the cracking load of B1 is 30% higher than that of B2. After B1 cracks, its deflection increases slowly, and its ductility is significantly improved. In addition, it does not show characteristics of brittle fracture that less-reinforced concrete often shows. This indicates that steel fibre can inhibit cracks in concrete from further extending and developing.

(3) Although total steel content in B1–B4 is the same, the working loads of B2 are 7% and 13% higher than those of B1 and B4, respectively. In addition, the ultimate load of B2 is 9% and 35% higher than those of B1 and B4, respectively. This indicates that the longitudinal rebar ratio at the bottom of the member determines its ultimate load, and the addition of steel fibre into concrete cannot improve its ultimate bearing capacity.

(4) Because there is a difference between the rebar reinforcement ratios of B1 and B4 in the compression zone, the working load and the ultimate load of B1 are different from those of B4. The working load and the ultimate load of B4 are 11% and 21% lower than those of B1. This indicates that when the compressive deformation of the compressive zone is significant, the bearing capacity of the member decreases, the foam concrete is crushed, and the member is destroyed.

(5) As long as the total steel content in B1–B4 is the same, the addition of steel fibre into concrete without rebar improves neither crack resistance nor ultimate bearing capacity of the member. In addition, when the volume fraction of steel fibre is 1.5%, the concrete exhibits the best mechanical performance. With further increase in the volume fraction of steel fibre, the bearing capacity cannot be improved.

(6) Although total steel content in B1–B4 is the same, both the occurrence and development of inclined cracks on the four experimental slabs are different. The reinforcement configuration (steel fibre and rebar) has an effect on the destruction of the oblique section. When the cracking load of the oblique section is reached, steel fibre can delay the opening of the inclined cracks. However, for steel fibre-reinforced concrete without a longitudinal rebar, inclined cracks appear even when the load is low.

(7) When total steel content in the slabs is the same, by an adjustment of the volume content of longitudinal rebar and steel fibre, the optimal cracking load, working load, and ultimate load of the slab can be achieved simultaneously. It is inferred that when we use steel fibre-rebar-reinforced concrete (volume fraction is 1.5%) with a longitudinal rebar ratio of no less than the minimum rebar reinforcement ratio as the tensile zone and use steel fibre-reinforced concrete (volume fraction is 1.5%) without rebar as the compression zone, the slab will attain its best performance.

Acknowledgements

This work was supported by the Ministry of Housing and Urban-Rural Development of China (Grant No. 2010-k1-26).

Conflict of Interests

The authors declare no conflicts of interest.

REFERENCES

1. di Prisco M, Plizzari G, Vandewalle L. Fibre reinforced concrete: new design perspectives. Mater Struct 2009;42(9):1261–81.
2. CECS 38:2004. Brief Introduction of Technical Specification for Fibre Reinforced Concrete Structures [S]. Beijing：China Planning Press，2004 (in chinese).
3. fib Bulletin 65, 2010. Model code 2010 – final draft, vol. 1; 2012. 350 pages.ISBN: 978-2-88394-105-2.
4. fib Bulletin 66, 2010. Model code 2010 – final draft, vol. 2; 2012. 370 pages.ISBN: 978-2-88394-106-9.
5. Smith Scott T, Hu Shenghua, Kim Seo Jin, Seracino Rudolf. FRP-strengthened RC slabs anchored with FRP anchors. Eng Struct 2011;33(4):1075–87.
6. Sorelli L, Meda A, Plizzari G. Steel fibre concrete slabs on ground: a structural matter. ACI Struct J 2006;103(4):551–8.
7. RILEM TC 162-TDF. Test and design methods for steel fibre reinforced concrete-r–e design method: final recommendations. Mater Struct 2003;36:560–7.
8. Destrée X. Free suspended elevated flat slabs of steel fibre reinforced concrete:full scale tests and design. In: 7th international RILEM-symposium on fibre reinforced concrete, Chennai. p. 941–50
9. Belletti, B., Cerioni, R., Meda, A., and Plizzari, G. (2008). Design aspects on steel fibre-reinforced concrete pavements. J. Mater. Civ.Eng.,10.1061/(ASCE)0899-1561(2008)20:9(599),599–607.
10. RILEM. (2002). Tests and design methods for steel fibre reinforced concrete: Design of steel fibre reinforced concrete using the σ–w method: Principles and applications. Mater. Struct.35(5), 262–278.
11. RILEM. (2003). Test and design methods for steel fibre reinforced concrete—σ–ε design method—Final recommendation.Mater.Struct., 36(8), 560–567.
12. Pujadas, P., Blanco, A., Cavalaro, S., and Aguado, A. (2014b). Plastic fibres as the only reinforcement for flat suspended slabs: Experimentalinvestigation and numerical simulation. Constr. Build. Mater.,57,92–104.
13. R. Al-Rousan, M. Issa, H. Shabila.Performance of reinforced concrete slabs strengthened with different types and configurations of CFRP. 2011 Elsevier Ltd. All rights reserved. doi:10.1016/j.compositesb.2011.08.050
14. Elgabbas F, El-Ghandour AA, Abdelrahman AA, El-Dieb AS. Different CFRP strengthening techniques for prestressed hollow core concrete slabs:experimental study and analytical investigation. Compos Struct

2010;92(2):401–11.
15. Laranjeira F, Grünewald S, Walraven J, Blom C, Molins C, Aguado A.Characterization of the orientation profile of steel fibre reinforced concrete.Mater Struct 2011;44(6):1093–111.
16. Ferrara L, Ozyurt N, di Prisco M. High mechanical performance of fibre reinforced cementitious composites: the role of "casting-flow induced" fibre orientation. Mater Struct 2011;44(1):109–28.
17. Luca Facconi , Fausto Minelli , Giovanni Plizzari. Steel fibre reinforced self-compacting concrete thin slabs – Experimental study and verification against Model Code 2010 provisions.Engineering Structures 122 (2016) 226–237
18. Yousheng Tao. Analysis on energy saving effect of aerated concrete building [J]. NEW BUILDING MATERIALS 2005(01) (in Chinese).
19. Zhouhong Zhang, Feng Liu, Lijuan Li, Yingqin Chen, Genyu Fan. The research and application of fibre reinforced concret [J]. NEW BUILDING MATERIALS 2003 (06) (in Chinese).
20. Michels J, Waldmann D, Maas S, Zürbes A. Steel fibres as only reinforcement for flat slab construction – experimental investigation and design. Constr Build Mater 2012;26(1):145–55. ISSN 0950-0618.
21. Michels J, Christen R, Waldmann D. Experimental and numerical investigation on postcracking behavior of steel fibre reinforced concrete. Eng FractMech 2013; 98:326–49. http://dx.doi.org/10.1016/j.engfracmech.2012.11.004.
22. Destrée X. Free suspended elevated flat slabs of steel fibre reinforced concrete:full scale tests and design. In: 7th international RILEM-symposium on fibrereinforced concrete, Chennai. p. 941–50.
23. Mobasher B, Yao Y, Soranakom C. Analytical solutions for flexural design of hybrid steel fibre reinforced concrete beams. Eng Struct 2015;100:164–77.ISSN 0141-0296.
24. Chiaia B, Fantilli A, Vallini P. Combining fibre-reinforced concrete with traditional reinforcement in tunnel linings. Eng Struct 2009;31(7):1600–6.
25. Pujadas P, Blanco A, De La Fuente A, Aguado A. Cracking behavior of FRC slabs with traditional reinforcement. Mater Struct/Mater Constr 2012;45(5):707–25.
26. Barros JAO, Taheri M, Salehian H. A model to simulate the moment–rotation and crack width of FRC members reinforced with longitudinal bars. Eng Struct 2015;100:43–56. http://dx.doi.org/10.1016/j.engstruct.2015.05.036. ISSN 0141-0296.
27. Alireza Gholamhoseini, Amir Khanlou,Gregory MacRae,Allan Scott, Stephen Hicks, Roberto Leon.An experimental study on strength and serviceability of reinforced and steel fibre reinforced concrete (SFRC) continuous composite slabs.Engineering Structures114(2016)171–180.
28. GB/T 50152-2012. Stanard for test method of concrete structures [S]. Beijing: China Architecture & Building Press, 2012 (in Chinese).
29. GB 50010-2010. Code for design of concrete structures [S]. Beijing: China Architecture & Building Press, 2010 (in Chinese).
30. Chujie Jiao, Wei Sun, Peizheng Gao, Yun Zhou. Experimental study on mechanical performance of steel fibre reinforced concrete [J]. Journal of Guangzhou University (Natural Science Edition), 2005(04) (in Chinese)
31. Guarded hot plate apparatus method for determination of steady-state thermal resistance and related properties of thermal insulation materials. National standards of the People's Republic of China. GB/T10294-2008/ISO 8302:1991.
32. Bo Yuan, Guangchuang Men. The design and thermal calculation of foam concrete sandwich panels [J]. Cryogenic building technology, 2015, 37 (11): 32-33.
33. Leilei Zhang, Wuxiang Wang. Research progress and application of foam concrete. [J]. building block and block building, 2010 (1): 38-42.

LIST OF FIGURES AND TABLES:

BADANIE DOŚWIADCZALNE WIELOROWKOWEJ, JEDNOKIERUNKOWEJ PŁYTY ZESPOLONEJ WYKONANEJ Z WŁÓKNA STALOWEGO, PIANKI I ZWYKŁEGO BETONU

Słowa kluczowe: włókno stalowe; beton piankowy; płyta wielorowkowa; płyta jednokierunkowa; płyta zespolona.

PODSUMOWANIE:

Dodanie włókna do betonu może zwiększyć odporność na pękanie, wytrzymałość na rozciąganie i sztywność. A zatem, beton zbrojony włóknem szklanym posiada wiele zastosowań inżynieryjnych jako rodzaj materiałów budowlanych, a ponadto istnieje wiele kodeksów zawierających wskazówki dotyczące jego konstrukcji. Beton zbrojony włóknem stalowym, otrzymywany poprzez dodanie losowo rozproszonego krótkiego włókna stalowego do betonu, jest rodzajem wieloskładnikowego materiału kompozytowego na bazie cementu. Ma dobre właściwości fizyczne i mechaniczne. Beton piankowy, który posiada wiele doskonałych właściwości, w tym lekkość i dobrą izolację termiczną, jest szeroko stosowany jako materiał ścienny, dachowy i podłogowy. Jednakże, ze względu na fakt, iż beton piankowy charakteryzuje się wysoką zdolnością pochłaniania wody, posiada słabą odporność na mrozy po wchłonięciu wody i może łatwo ulegać pęknięciu podczas cykli zamrażania i rozmrażania, co wpływa na funkcję i wygląd zewnętrzny budynku. Natomiast beton zbrojony włóknem stalowym charakteryzuje się dobrą odpornością na pękanie i nieprzepuszczalnością. Dlatego też, łącząc zalety betonu zbrojonego włóknem stalowym (dobra nieprzepuszczalność) z wielorowkową strukturą (dobre właściwości mechaniczne), zaprojektowaliśmy nowy rodzaj wielorowkowej, prefabrykowanej płyty zespolonej. Celem niniejszej pracy jest zbadanie wpływu konfiguracji zbrojenia (włókna stalowego i pręta zbrojeniowego) na właściwości mechaniczne płyt zespolonych o takiej samej zawartości stali. Wyprodukowaliśmy cztery kawałki pełnowymiarowych, wielorowkowych, prefabrykowanych płyt zespolonych o różnych konfiguracjach zbrojenia, z wykorzystaniem betonu zbrojonego włóknem stalowym, betonu piankowego i zwykłego betonu. Wielorowkowa, zespolona, prefabrykowana płyta posiada wiele doskonałych właściwości, takich jak lekkość, dobra izolacja termiczna i akustyczna, itp. W związku z tym, może być ona stosowana na wytworzonej konstrukcji. Ponadto, zbadano zespolone, prefabrykowane płyty o takiej samej zawartości stali, lecz różnych konfiguracjach zbrojenia, pod takim samym obciążeniem statycznym i uzyskano wiele wskaźników technicznych, takich jak odporność na pękanie, obciążenie plastyczne, maksymalna nośność, maksymalne ugięcie, destrukcyjny wzór oraz naprężenie stalowych prętów zbrojeniowych. Wyniki pokazują, że konfiguracja zbrojenia ma znaczący wpływ na właściwości mechaniczne zespolonych, prefabrykowanych płyt o takiej samej zawartości stali, a zespolona, prefabrykowana płyta zbrojona podłużnym prętem zbrojeniowym i włóknem stalowym (ułamek objętościowy wynosi 1,5%) charakteryzuje się najlepszymi parametrami mechanicznymi i plastycznością.

Proces wytwarzania płyty zespolonej jest bardziej skomplikowany niż w przypadku zwykłej płyty betonowej. Płyta zespolona charakteryzuje się jednak dobrą wydajnością mechaniczną, wysoką odpornością na pękanie, dobrą izolacją termiczną, niskimi kosztami eksploatacji i konserwacji, które spełniają wymagania w zakresie uprzemysłowienia elementów konstrukcyjnych, efektywności energetycznej budynków i budownictwa ekologicznego. Tak więc, pomimo złożonego procesu produkcyjnego, ten rodzaj płyty zespolonej ma jasne perspektywy rynkowe i szerokie zastosowania.